CrossMark

J. Fluid Mech. (2015), *vol.* 782, *pp.* 356–367. © Cambridge University Press 2015
doi:10.1017/jfm.2015.542

Asymptotic descriptions of oblique coherent structures in shear flows

Kengo Deguchi[1,†] **and Philip Hall**[2,†]

[1]Department of Mathematics, Imperial College London, South Kensington Campus, London SW7 2AZ, UK

[2]School of Mathematics, Monash University, Melbourne, VIC 3800, Australia

(Received 17 February 2015; revised 24 July 2015; accepted 10 September 2015; first published online 8 October 2015)

Exact coherent states in plane Couette flow are extended to an oblique parallelogram computational domain and the large-Reynolds-number asymptotic descriptions of the states are derived. When the tilt angle of the domain is increased, the states first obey vortex–wave interaction theory and then develop a new asymptotic structure. The latter asymptotic structure is characterized by a self-similar nonlinear interaction localized in the fluid layer. For the largest scale of the self-similar nonlinear structure, the theory predicts an inverse Reynolds number dependence for the tilt angle of the oblique pattern. That result is consistent with the numerical and experimental observations of the laminar–turbulent banded pattern in shear flows.

Key words: instability, nonlinear instability, transition to turbulence

1. Introduction

The emergence of the quasi-coherent oblique laminar–turbulent banded patterns in shear flows has long been recognized since the early Taylor–Couette flow experiments by Coles (1965) and more recently by Prigent *et al.* (2002). The formation of the banded pattern generally occurs in various subcritical shear flows; for example, the pattern has been numerically found for plane Couette flow by Barkley & Tuckerman (2005) and plane Poiseuille flow by Tsukahara, Seki & Tochio (2005). However, the physical mechanism behind the sustainment of such a coherent banded pattern has not been established.

In the shear-flow-transition literature, coherent structures consisting of streaks and rolls have been related to numerically obtained exact solutions of the Navier–Stokes equations. Such solutions, typically found in a pair of upper and lower branch states, were first discovered by Nagata (1990) for plane Couette flow and then subsequently called exact coherent structures by Waleffe (1997).

On the other hand, for high Reynolds numbers and $O(1)$ wavelengths, Hall & Sherwin (2010) conclusively showed that the lower branch exact coherent states in plane Couette flow are described by the vortex–wave interaction theory of Hall & Smith (1991). The theory was further extended to upper branch states by Deguchi & Hall (2014*a*), to long streamwise wavelengths by Deguchi, Hall & Walton (2013) and

† Email addresses for correspondence: k.deguchi@imperial.ac.uk, phil.hall@monash.edu

https://doi.org/10.1017/jfm.2015.542 Published online by Cambridge University Press

to unbounded shear flows by Blackburn, Hall & Sherwin (2013) and Deguchi & Hall (2014*b*). Various asymptotic states found by these authors described the parameter dependence of the exact coherent states. Here we remark that these theories are not reliant on any modelling argument to ignore certain terms in the governing equations, thereby explaining the minimum mechanism of the self-sustainment nature of coherent states in a rational way.

In this paper, we are concerned with the generalization of the asymptotic theories to the oblique banded patterns observed in the experiments and direct numerical simulations. For definiteness we choose plane Couette flow as a model but the results in this paper have a broad applicable range, as for already developed asymptotic theories. In the next section we begin the analysis by formulating the full Navier–Stokes problem which we will solve numerically. A computational box inclined in the streamwise direction is used to compute oblique exact coherent states. The numerical results are summarized in § 3. The results are consistent with high-Reynolds-number asymptotic theories developed in the same section. Finally, in § 4, we draw some conclusions.

2. Formulation of the problem

In Cartesian coordinates $[x, y, z]$, we seek steady solutions of plane Couette flow governed by incompressible Navier–Stokes equations:

$$[u\partial_x + v\partial_y + w\partial_z]\begin{bmatrix} u \\ v \\ w \end{bmatrix} = -\begin{bmatrix} \partial_x p \\ \partial_y p \\ \partial_z p \end{bmatrix} + Re^{-1}[\partial_x^2 + \partial_y^2 + \partial_z^2]\begin{bmatrix} u \\ v \\ w \end{bmatrix}, \tag{2.1a}$$

$$\partial_x u + \partial_y v + \partial_z w = 0, \tag{2.1b}$$

$$[u, v, w] = [\pm 1, 0, 0] \quad \text{at } y = \pm 1, \tag{2.1c}$$

where Re is the Reynolds number and we have non-dimensionalized the equations so that the half-gap, wall speed and density are to be unity.

In the computational community these equations have usually been solved together with periodic conditions in x, z. However, Barkley & Tuckerman (2005) showed that a rectangular periodic box oriented in the direction of the band is a more natural periodic computational domain for the oblique banded pattern. The strategy we adopt here is inspired by their work but the numerical implementation is closer to Deguchi & Altmeyer (2013), which facilitates the derivation of the asymptotic theories in the later sections. The benefit we will receive from the latter approach is that we can choose the streamwise and spanwise wavelengths independently of the tilt angle of the oblique domain. Notice that we can also construct similar asymptotic theories in the rectangular domain to those used by Barkley & Tuckerman (2005), although the streamwise and spanwise wavelengths are now functions of the tilt angle and thus the theories may become complicated.

In oblique coordinates,

$$\xi = x, \quad \zeta = -\alpha\gamma x + z, \tag{2.2a,b}$$

we apply periodic conditions of the form

$$[\boldsymbol{u}, p](\xi, y, \zeta) = [\boldsymbol{u}, p](\xi + 2\pi/\alpha, y, \zeta), \tag{2.3a}$$

$$[\boldsymbol{u}, p](\xi, y, \zeta) = [\boldsymbol{u}, p](\xi, y, \zeta + 2\pi/\beta), \tag{2.3b}$$

https://doi.org/10.1017/jfm.2015.542 Published online by Cambridge University Press

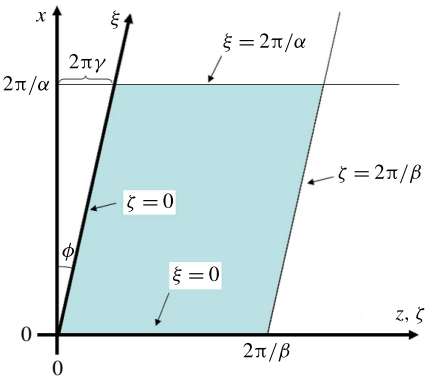


FIGURE 1. (Colour online) Schematic of the computational domain.

to define a parallelogram-shaped periodic domain, pictured in figure 1. The shape of the domain is determined by the wavenumbers α, β and the tilt parameter γ. The tilt angle of the domain is defined by $\phi = \arctan(\alpha\gamma)$. In the new coordinates the differential operators ∂_x and ∂_z in (2.1) must be replaced by $\partial_\xi - \alpha\gamma\partial_\zeta$ and ∂_ζ, respectively.

In order to solve the nonlinear equations, the Galerkin spectral code developed in Deguchi *et al.* (2013) for Cartesian coordinates is used as the basis of the numerical scheme. The code uses a toroidal–poloidal potential decomposition to simplify the problem. These potentials are first expanded by modified lth-order Chebyshev polynomials in y, and then each Chebyshev spectrum coefficient a_l is further decomposed into Fourier series as

$$a_l(x, z) = \sum_{m,n} \hat{a}_{lmn} \exp[\mathrm{i}(m\alpha x + n\beta z)] + \text{c.c.}, \tag{2.4}$$

where c.c. stands for complex conjugate. Instead of (2.4), following Deguchi & Altmeyer (2013), here we use the expansion

$$a_l(\xi, \zeta) = \sum_{m,n} \hat{a}_{lmn} \exp[\mathrm{i}(m\alpha - n\alpha\beta\gamma)x + \mathrm{i}n\beta z] + \text{c.c.} \tag{2.5}$$

to compute solutions in a parallelogram-shaped domain. The algebraic equations for the unknown spectral coefficients resulting from a Galerkin projection are solved by using Newton's method. The convergence criterion used here is the same as that used in Deguchi & Hall (2014*a*). Note that the limit of $\gamma \to 0$ recovers the Cartesian case.

3. Numerical results and high-*Re* asymptotic theories

In order to obtain solutions for $\gamma > 0$, we use a homotopy continuation of the solution branch from the mirror-symmetric solutions found by Gibson, Halcrow & Cvitanovic (2009) and Itano & Generalis (2009) for $\gamma = 0$. For wavenumbers $(\alpha, \beta) = (0.75, 1.37)$, which we use throughout the paper, this solution arises as a saddle–node bifurcation at $Re \approx 140$ creating lower and upper branches; these branches are called EQ7 and EQ8 respectively in the latter paper. The solutions have symmetries

$$[u, v, w](x, y, z) = [u, v, -w](x + \pi/\alpha, y, -z), \tag{3.1a}$$

$$[u, v, w](x, y, z) = [-u, -v, -w](-x, -y, -z), \tag{3.1b}$$

$$[u, v, w](x, y, z) = [u, v, w](x + \pi/\alpha, y, z + \pi/\beta). \tag{3.1c}$$

https://doi.org/10.1017/jfm.2015.542 Published online by Cambridge University Press

In general, if the symmetry (3.1*a*) is present there must be zero spanwise mean flow correction, $w_m = \overline{w}$, which is defined by the averaging operator

$$\overline{*} = \frac{\alpha\beta}{4\pi^2}\int_0^{2\pi/\alpha}\int_0^{2\pi/\beta} * \,\mathrm{d}x\,\mathrm{d}z. \tag{3.2}$$

Also, we note that the solutions are steady, if they satisfy (3.1*b*).

When γ is increased from zero, any symmetry which involves reflection in z is destroyed. This means that the shift–reflection symmetry (3.1*a*) of the solution breaks and a spanwise mean flow must be produced. However, the symmetries (3.1*b*) and (3.1*c*) do not break, and thus the solution remains steady. Note that steady solutions with spanwise mean flow have already been reported in Gibson *et al.* (2009). Those solutions, classified as EQ9–EQ13, also satisfy (3.1*b*) but not (3.1*a*) and (3.1*c*).

The results obtained by gradually increasing γ are shown in figure 2(*a*). The streamwise wall shear correction of the solution $\Delta_u = (\mathrm{d}u_m/\mathrm{d}y)|_{y=1}$, defined by the streamwise mean flow correction $u_m = \overline{u} - y$, is used as a measure of the solutions. The solution branches for $Re = 350$, 1000, 10 000, 20 000, 30 000 and 40 000 are shown in the figure. For relatively large Re, first Δ_u increases when γ is increased from zero and then reaches a maximum. The maximum points shift to smaller γ with increasing Re. The numerical results indicate that the value of γ at the maximum scales like Re^{-1}, as shown in figure 2(*b*); see the arrow in the figure which indicates the position of the maximum. After the maximum point, Δ_u decreases with increasing γ. For large γ a new scaling emerges: we find $\gamma \sim Re^{-1/3}$, $\Delta_u \sim Re^{-2/3}$ which leads us to an asymptotic scaling valid even for Re as low as 350; see figure 2(*c*). The following subsections describe these asymptotic behaviours using high-Reynolds-number asymptotic theories.

3.1. *The vortex–wave interaction stage*

For $\gamma = 0$, Deguchi & Hall (2014*b*) showed that with increasing Re the lower branch mirror-symmetric mode solutions become vortex–wave interaction states, VWI for short. These states were derived by Hall & Smith (1991) and first applied to plane Couette flow by Hall & Sherwin (2010). The VWI theory has a deep relevance to the self-sustaining process picture of how exact coherent structures hold together. The self-sustaining process description was derived by Waleffe (1997) by a numerical interrogation of solutions of the Navier–Stokes equations. That interrogation showed how streamwise periodic waves occur as instabilities of a streak process but drive rolls through the Reynolds stress terms in the Navier–Stokes equations. The roll then drives the streak, thereby closing the process. In Hall & Smith (1991) the high-Reynolds-number description of that process had previously been explicitly derived in the context of boundary layer flows. Subsequently Hall & Sherwin (2010) showed, in the context of plane Couette flow, that the mechanism driving the rolls is essentially a steady streaming process involving a wave concentrated in its critical layer driving a streamwise-averaged flow. The self-sustained process picture was derived at finite Reynolds numbers and it is only because the VWI description turns out to apply at relatively low Reynolds number that the separation of individual processes was possible.

Following the VWI theory, now let us decompose the flow field into the vortex and wave components. The vortex component usually refers to the streamwise-averaged

https://doi.org/10.1017/jfm.2015.542 Published online by Cambridge University Press

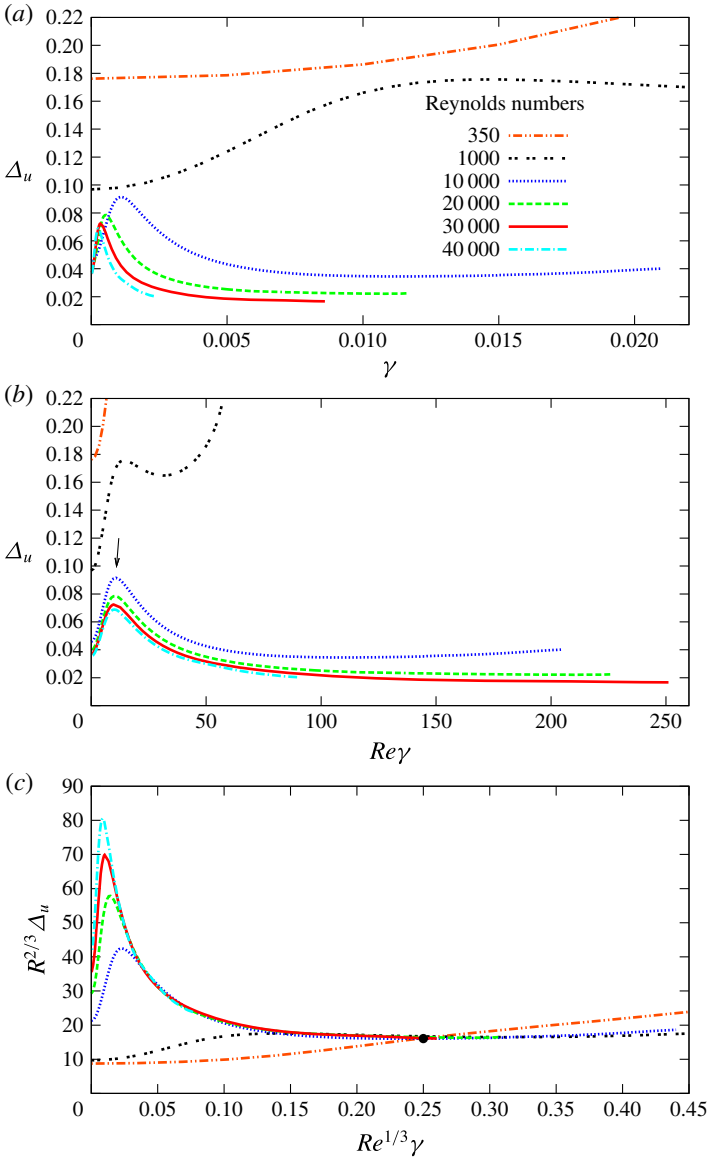


FIGURE 2. (Colour online) The change of the drag of the oblique exact coherent structures as a function of the tilt parameter for $(\alpha, \beta) = (0.75, 1.37)$. To draw the diagrams, 100–110 Chebyshev modes are used in y whilst 4–14 and 28–52 Fourier modes are used in ξ and ζ, respectively. The arrow in (b) indicates the maximum of the drag.

flow field, but here we define this component by averaging in ξ and are concerned with how much we can increase the angle of this vortex component from the principal direction of the basic flow. Therefore, using the classical VWI scalings in Cartesian coordinates, we expand in the form

$$u = U + \rho(\tilde{u}e^{i\alpha\xi} + \text{c.c.}) + \cdots, \tag{3.3a}$$

$$v = Re^{-1}V + \rho(\tilde{v}e^{i\alpha\xi} + \text{c.c.}) + \cdots, \tag{3.3b}$$

https://doi.org/10.1017/jfm.2015.542 Published online by Cambridge University Press

$$w = Re^{-1}W + \rho(\tilde{w}\mathrm{e}^{\mathrm{i}\alpha\xi} + \text{c.c.}) + \cdots, \tag{3.3c}$$

$$p = Re^{-2}P + \rho(\tilde{p}\mathrm{e}^{\mathrm{i}\alpha\xi} + \text{c.c.}) + \cdots, \tag{3.3d}$$

where $[U, V, W, P](y, \zeta) \in \mathbb{R}$ and $[\tilde{u}, \tilde{v}, \tilde{w}, \tilde{p}](y, \zeta) \in \mathbb{C}$ are the vortex and wave components, respectively. Hereafter we refer to U and (V, W) as streak and roll, respectively. The scaling for the roll–streak components follows from the usual Taylor-vortex scaling that allows the viscous effect to be present in the whole channel; see Taylor (1923) for example. On top of the roll–streak a wave of unknown amplitude propagates. The size of the wave, $\rho \ll Re^{-1}$, is to be fixed in terms of Re so that it drives the vortex by inducing a stress jump across the critical layer.

The leading-order equations for the vortex component are

$$[V\partial_y + (W - \alpha\gamma_0 U)\partial_\zeta] \begin{bmatrix} U \\ V \\ W \end{bmatrix} = - \begin{bmatrix} 0 \\ \partial_y P \\ \partial_\zeta P \end{bmatrix} + [\partial_y^2 + \partial_\zeta^2] \begin{bmatrix} U \\ V \\ W \end{bmatrix}, \tag{3.4a}$$

$$\partial_y V + \partial_\zeta (W - \alpha\gamma_0 U) = 0, \tag{3.4b}$$

where we have written $\gamma = Re^{-1}\gamma_0$ to remove Re from the equations. The Re^{-1} scaling of γ follows from the relative size of the roll and streak. The scaling determines an appropriate angle between the directions of the basic flow and the viscous roll–streak, and has a close relationship to the work of Hall (1985) on the Görtler vortex problem in three-dimensional boundary layers.

The leading-order wave equations satisfy the inviscid equations linearized around the streaky field $[U, 0, 0]$ that can be transformed into a generalized Rayleigh equation:

$$\left(\partial_y^2 + \partial_\zeta^2 - \alpha^2 - 2\frac{\partial_y U}{U}\partial_y - 2\frac{\partial_\zeta U}{U}\partial_\zeta\right)\tilde{p} = 0. \tag{3.5}$$

The Rayleigh equation (3.5) is singular at the critical layer $y = f(\zeta)$ where $U(f(\zeta), \zeta) = 0$ so we need a separate analysis there. In order to regularize the equation we need to bring back viscosity and the viscous–convective balance gives the classical critical layer thickness $\delta_c = Re^{-1/3}$. From the local expansion around the critical layer the wave velocity component tangential to the critical layer, say $\tilde{v}^s$, must increase by a factor of δ_c^{-1}. Then the wave creates a Reynolds stress in the critical layer which balances the viscous term in the vortex system. Integrating the vortex equations across the critical layer, we can find that the stress jump drives the roll flow. The unknown wave size ρ is then fixed by making that jump of $O((Re\tilde{v}^s)^2\delta_c)$, comparable to the $O(1)$ roll stresses outside of the critical layer. From that balance we deduce $\rho = Re^{-7/6}$.

The critical layer equations derived in this way are exactly the same as the Cartesian case on replacing (x, y) by (ξ, ζ). Therefore, as shown in Hall & Sherwin (2010), switching from (y, ζ) to the body-fitted coordinates (n, s), where n and s represent the normal and tangential coordinates along the critical layer, the stress jump of the roll component can be analytically solved as

$$[\partial_n V^s]_-^+ = n_0\alpha^{-5/3}\partial_s(\mu^{-5/3}|\partial_s\tilde{p}|^2), \tag{3.6a}$$

$$[P]_-^+ = -n_0(\alpha\mu)^{-5/3}\Lambda_0|\partial_s\tilde{p}|^2, \tag{3.6b}$$

where $V^s(n, s)$ is the roll velocity tangential to the critical layer, $\mu = (\partial_n U)|_{y=f}$ is the streak shear evaluated on the critical layer, Λ_0 is the critical layer curvature, and

https://doi.org/10.1017/jfm.2015.542 Published online by Cambridge University Press

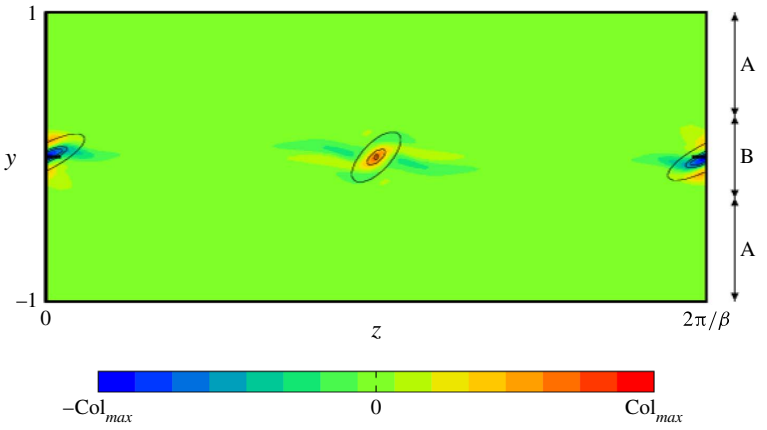


FIGURE 3. (Colour online) The streamwise vorticity $\omega = (\partial_z v - \partial_y w)$ of the nonlinear solutions at $x = 0$ for $(\alpha, \beta, \gamma) = (0.75, 1.37, 0.25Re^{-1/3})$. Colour represents the localization of flow structure at the filled circle in figure 2(*c*) where $Re = 30\,000$ and $\mathrm{Col}_{max} = 0.0849$. The three ovals placed at each localized structure represent 60 % maximum of $|\omega|$ for $Re = 1000$, 10 000 and 30 000, from outside to inside.

$n_0 = 2\pi(2/3)^{2/3}\Gamma(1/3)$. The jump closes the problem and (3.4)–(3.6) constitute a self-consistent set of equations formally derived from the Navier–Stokes equations in the limit $Re \to \infty$.

The above discussion clearly shows that the VWI theory is still valid for $\gamma \sim O(Re^{-1})$, consistent with figure 2(*b*). The overall interaction scenario does not change from the usual VWI; the tilt angle just controls the vortex advection by the streak field in (3.4), and does not influence the structure of the wave system (3.5) and the jump conditions (3.6). In this VWI regime, the streamwise wall shear correction Δ_u is $O(1)$ whilst the spanwise wall shear Δ_w, defined by $(\mathrm{d}w_m/\mathrm{d}y)|_{y=1}$, is $O(Re^{-1})$. Note that our result here also supports the conclusion by Deguchi & Hall (2014*b*) that the large-Reynolds-number mirror-symmetric mode is of VWI type.

3.2. *The boundary region equations*

In the last subsection we saw that when γ becomes larger than $O(Re^{-1})$ the VWI structure breaks down. The breakdown process, which we shall concentrate on here, is similar to that observed in Deguchi *et al.* (2013), where a long streamwise wavelength of $O(Re)$ is considered. The key point of the theory is that the critical layer spreads out to fill the whole channel so that we have a regular behaviour everywhere in the flow. The outcome of the spreading is that the vortex and wave components are comparable in size and it is not possible to distinguish between these quantities. In Deguchi *et al.* (2013), the long-wavelength asymptotic states were found to be governed by the so-called boundary-region equations (BREs), instead of the VWI system (3.4)–(3.6). The BREs are given by (2.1*a*) and (2.1*b*) with unit Re and ∂_x neglected on the right-hand side of (2.1*a*). However, because now we fix the streamwise wavelength to be of $O(1)$, there are several fundamental differences.

In order to find the asymptotic structure observed in figure 2(*c*), we first examine the numerically obtained flow properties. Figure 3 shows the streamwise vorticity ω of the oblique exact coherent states for $\gamma = 0.25Re^{-1/3}$ in a y–z cross-section at $x = 0$.

https://doi.org/10.1017/jfm.2015.542 Published online by Cambridge University Press

The colour in the figure shows that the vortex structure is localized in y, similar to the unbounded VWI. Moreover, the structure is also localized in z; in fact, the tails of the localized structure exponentially decay as observed by Gibson & Brand (2014). We observe that the localized structure shrinks in both y and z with increasing Re. Two families of three superimposed ovals in the figure are 60 % maximum of $|\omega|$ for $Re = 1000$, 10 000 and 30 000. This property highlights a physical difference from the VWI case where roll–streak components occupy the whole channel. Also, in contrast to VWI, the states governed by BREs could possess a complicated streamwise dependence; recall that the streamwise dependence of the VWI states is dominated by a monochromatic Rayleigh neutral wave. Detailed visualizations of the VWI states can be found in Hall & Sherwin (2010), Blackburn *et al.* (2013) and Deguchi & Hall (2014*a*,*b*).

In view of the observation above we scale (y, ζ) as $y = \epsilon Y$ and $\zeta = \epsilon Z$ with a small parameter ϵ to be specified later. We then expand the flow field as

$$u = Re^{-1}\epsilon^{-2}U(\xi, Y, Z) + Re^{-1}\epsilon^{-1}U_1(\xi, Y) + Re^{-1}d_u Y + \cdots, \tag{3.7a}$$

$$v = Re^{-1}\epsilon^{-1}V(\xi, Y, Z) + Re^{-1}V_1(\xi, Y) + \cdots, \tag{3.7b}$$

$$w = Re^{-1}\epsilon^{-1}W(\xi, Y, Z) + Re^{-1}W_1(\xi, Y) + \epsilon Re^{-1}d_w Y + \cdots, \tag{3.7c}$$

$$p = Re^{-2}\epsilon^{-2}P(\xi, Y, Z) + Re^{-2}\epsilon^{-1}P_1(\xi, Y) + \cdots, \tag{3.7d}$$

and seek a nonlinear solution in a layer of depth $O(\epsilon)$, i.e. the layer 'B' in figure 3. The size of the leading-order spanwise-averaged disturbance component, denoted by subscript 1, must be ϵ times smaller than the other leading-order terms, because the Reynolds stress driving this component is $O(\epsilon)$ times smaller than that for the other component due to the spanwise localization. Therefore the spanwise average of $[U, V, W]$ must be the 'basic' flow $[Y, 0, 0]$. The constants d_u and d_w appearing in the smaller-order terms are to be determined by the second-order spanwise-averaged flow problem. Substituting the above expansions into the scaled Navier–Stokes equations, we obtain a modified form of the BREs to leading order:

$$[U\partial_\xi + V\partial_Y + (W - \alpha\gamma_0 U)\partial_Z]\begin{bmatrix} U \\ V \\ W \end{bmatrix} = -\begin{bmatrix} 0 \\ \partial_Y P \\ \partial_Z P \end{bmatrix} + [\partial_Y^2 + \partial_Z^2]\begin{bmatrix} U \\ V \\ W \end{bmatrix}, \tag{3.8a}$$

$$\partial_\xi U + \partial_Y V + \partial_Z(W - \alpha\gamma_0 U) = 0, \tag{3.8b}$$

$$[U, V, W] \to [Y, 0, 0] \quad \text{as } Y \to \pm\infty, \tag{3.8c}$$

where we write $\gamma = \epsilon\gamma_0$ in order to balance the effect of the inclination of the domain. Equations (3.8) must be solved with periodic conditions in ξ and exponentially decaying conditions in Z for the disturbance. Thus we do not need to consider the spanwise-averaged part of these leading-order equations. This is the first difference from Deguchi *et al.* (2013), where the periodic condition is considered in the asymptotic problem, although they reported spanwise localized numerical solutions. The second difference is in the boundary conditions in Y that imply we are seeking a solution in an unbounded domain such as the unbounded VWI problem formulated by Blackburn *et al.* (2013) and Deguchi & Hall (2014*b*). The origin of the vertical localization is that we need a short vertical length scale to recover the regularity of the wave equation when the streamwise wavelength is restricted to be of $O(1)$. Outside of the interaction layer, the regions 'A' in figure 3, all of the disturbances decay except for the mean flow corrections which must take the form of an unforced

https://doi.org/10.1017/jfm.2015.542 Published online by Cambridge University Press

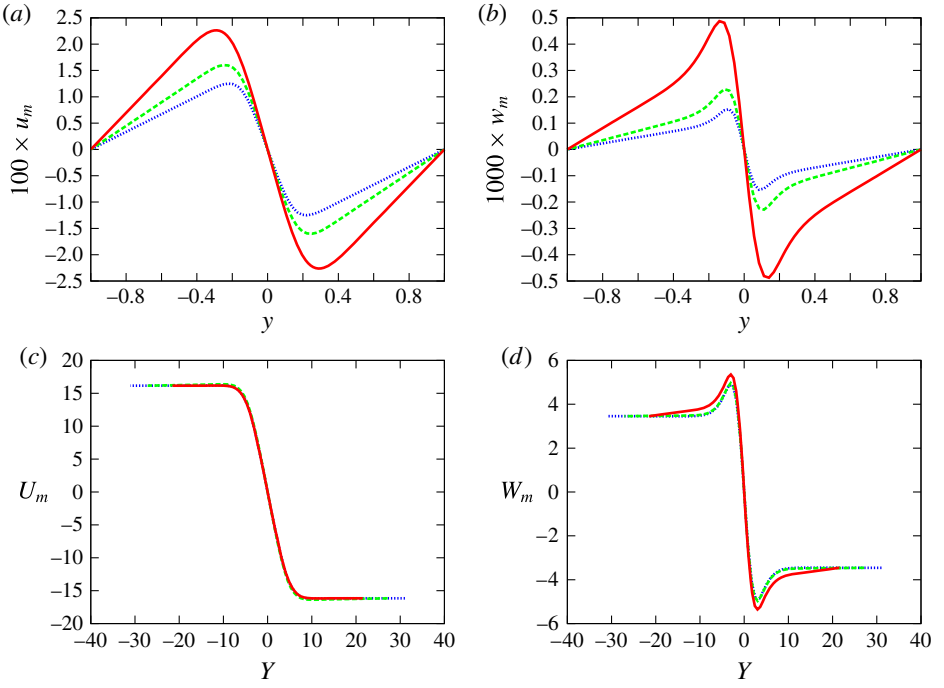


FIGURE 4. (Colour online) The mean flow correction of the nonlinear Navier–Stokes solutions for $(\alpha, \beta, \gamma) = (0.75, 1.37, 0.25Re^{-1/3})$: (a,b) non-scaled quantities u_m and w_m; (c,d) scaled quantities $U_m = Re^{2/3}u_m - Re^{-1/3}d_u Y$ and $W_m = Rew_m - Re^{-1/3}d_w Y$ in the expansion (3.7), where displacement velocities are $d_u = 16.16$ and $d_w = 3.456$. Red solid, green dashed and blue dotted lines are for $Re = 10\,000$, $20\,000$ and $30\,000$, respectively.

linear profile. Since U matches to the basic flow component y at large $|Y|$, we require $Re^{-1}\epsilon^{-2}Y = y = \epsilon Y$, i.e. $\epsilon = Re^{-1/3}$.

The components $[U_1, V_1, W_1]$ and P_1 are determined by the spanwise-averaged equations

$$\langle VU \rangle = \partial_Y^2 U_1, \quad \langle V^2 \rangle = -\partial_Y P_1 + \partial_Y^2 V_1, \tag{3.9a,b}$$

$$\langle VW \rangle = \partial_Y^2 W_1, \quad \partial_\xi U_1 + \partial_Y V_1 = 0, \tag{3.9c,d}$$

$$[U_1, V_1, W_1] \to [\mp d_u, 0, \mp d_w] \quad \text{as } Y \to \pm\infty, \tag{3.9e}$$

where $\langle * \rangle = \lim_{L\to\infty}(1/L)\int_0^L * \mathrm{d}Z$. The constants d_u and d_w are the displacement velocities in the mean flows $U_m(Y) = \overline{U}_1$ and $W_m(Y) = \overline{W}_1$ produced as a result of nonlinear interactions. These components, and smaller linear terms $Re^{-1}d_u$ and $\epsilon Re^{-1}d_w$ in (3.7), match to the unforced mean flow corrections of the linear profile outside of the interaction layer. The matching process is similar to that found in Deguchi & Hall (2014*b*). Since the mean flow corrections must be written in the form of $u_m \approx \Delta_u(y \mp 1)$ and $w_m \approx \Delta_w(y \mp 1)$ in the region 'A', the matching conditions yield $u_m = Re^{-1}\epsilon^{-1}d_u(y \mp 1)$ and $w_m = Re^{-1}d_w(y \mp 1)$. Therefore, the wall shears and displacement velocities are $\Delta_u = Re^{-2/3}d_u$ and $\Delta_w = Re^{-1}d_w$.

In order to confirm the asymptotic structure, we plot the streamwise and spanwise mean flow corrections from the full Navier–Stokes calculation for $Re = 10\,000$, $20\,000$

https://doi.org/10.1017/jfm.2015.542 Published online by Cambridge University Press

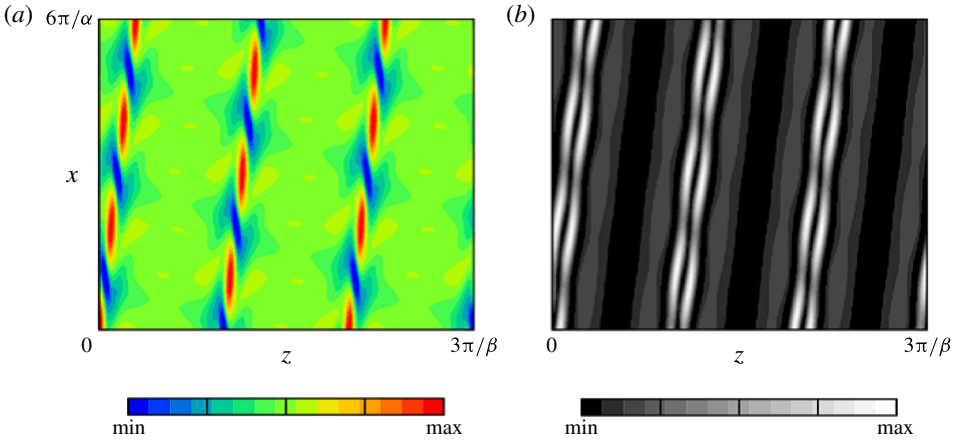


FIGURE 5. (Colour online) The asymptotically converged solution scaled for $Re = 350$. The solution shown in figure 3 is used for the asymptotic extrapolation. (*a*) Streamwise vorticity at $y = 0$, (*b*) kinetic energy $(u^2 + v^2 + w^2)/2$ at $y = 0$.

and 30 000 in figure 4(*a*,*b*). When we apply the scaling $U_m = Re^{2/3}u_m - Re^{-1/3}d_u Y$ and $W_m = Rew_m - Re^{-1/3}d_w Y$ to the mean flows, as shown in figure 4(*c*,*d*), the scaled mean flows converge to a single curve with increasing Re. Consistent with the theory, for large $|Y|$ the streamwise and spanwise scaled mean flows become the constant displacement velocities, $\pm d_u = 16.16$ and $\pm d_w = 3.456$, respectively, calculated by the wall shears.

We recall that the BREs scaling in figure 2(*c*) gives a better agreement of the $Re = 350$ curve with the asymptotically converged large-Re results compared with figure 2(*a*,*b*). Thus for relatively small Re it would be sensible to use BREs to describe oblique patterns. If the solution obtained for $Re = 30\,000$ is considered to be a good approximation to the solution of the reduced problem (3.8), we can use it to predict the behaviour of the oblique exact coherent structures for various values of Re. For definiteness, here we consider such a prediction for $Re = 350$ to compare with the simulation by Barkley & Tuckerman (2005). By increasing the tilt angle by a factor of $(30\,000/350)^{1/3}$ and extending the flow regime in the spanwise direction by the same factor as from the solution shown in figure 3, we have a prediction for the vorticity distribution at the mid-channel as shown in figure 5(*a*). In the figure, we can clearly see an oblique band structure localized in the spanwise direction.

The corresponding kinetic energy at the mid-plane of this regime is presented in figure 5(*b*). The region where the energy is highest is visualized by the small bright blobs aligned in oblique fashion and is seen to be similar to those observed in figures 1 and 5 of Barkley & Tuckerman (2005). However, in the simulation many blobs are clustered to create a large-scale laminar–turbulent band structure, whilst in our case the oblique band is created by a single line of localized blobs. This means that further computations are required before we reach a definitive conclusion. Here we remark that the difference could be resolved if we assume that the asymptotic equations can support more complicated asymptotic solutions which play a more important role in the dynamics. Thus one of the possible scenarios would be for the reduced system (3.8) to have solutions with clustered blobs connected by snakings of the solution branch similar to Schneider, Gibson & Burke (2010) or Deguchi & Hall (2014*a*). Alternatively a direct comparison with numerical simulations for

https://doi.org/10.1017/jfm.2015.542 Published online by Cambridge University Press

various Reynolds numbers could be used to validate our theory. Also, notice that the difference of the shape of the domains is not a significant issue in the comparison because the domains used both in this work and in Barkley & Tuckerman (2005) are appropriate periodic boxes to describe the minimum structure of the banded patterns, which are self-organized in large computational domains.

Once we have the solution of (3.8) for some α, an asymptotic solution with a different value of wavenumber, say $\hat{\alpha}$, can be easily obtained following a self-similar transformation similar to that proposed for unbounded VWI by Blackburn *et al.* (2013):

$$U = a^{1/3}\hat{U}, \quad V = a^{-1/3}\hat{V}, \quad W = a^{-1/3}\hat{W}, \quad P = a^{-2/3}\hat{P}, \tag{3.10a–d}$$

$$\xi = a\hat{\xi}, \quad Y = a^{1/3}\hat{Y}, \quad Z = a^{1/3}\hat{Z}, \quad \gamma_0 = a^{1/3}\hat{\gamma}_0, \tag{3.10e–h}$$

where $a = \hat{\alpha}/\alpha$. It is easy to confirm that the hat variables satisfy the same problem as (3.8) with a wavenumber $\hat{\alpha}$ in $\hat{\xi}$. We can increase the value of a until the nonlinear interaction layer of depth $\delta = O(a^{1/3}Re^{-1/3})$ fills the entire gap. For maximum $a \sim O(Re)$, the streamwise wavenumber is $\alpha \sim O(Re^{-1})$ and the same long-wavelength problem as discussed in Deguchi *et al.* (2013) is recovered if $\hat{\gamma}_0 = 0$. The tilt angle predicted for this largest-scale case, where the kinetic energy at the mid-plane is the most significant, is $\tan\phi = \alpha\gamma \sim O(\alpha^{2/3}Re^{-1/3}) \sim O(Re^{-1})$.

4. Conclusion

We have continued the solution branch of the mirror-symmetric exact coherent states in plane Couette flow to parallelogram-shaped computational domains. When the tilt angle of the domain ϕ is increased, we find that the solution develops into an oblique banded pattern. Our results for large Re were used to motivate asymptotic analyses which explained the parameter dependence of the results.

For small ϕ the oblique exact coherent states first obey the modified VWI theory satisfying $\tan\phi \sim O(Re^{-1})$ scaling. The scaling, obtained by considering the advection balance due to the roll and streak components, is consistent with Barkley & Tuckerman (2007), where the oblique banded pattern observed in the experiments and simulations is summarized. Good convergence of the numerical solutions to this asymptotic result are observed for relatively large Re of $O(10^4)$.

When the tilt angle of the domain is further increased, the solution eventually develops a localized structure in both spanwise and wall-normal directions. A new asymptotic theory was developed for this regime and it is found that the centre of the nonlinear interaction at the localized position is governed by the modified boundary-region equations. That situation is similar to the long-wavelength VWI theory by Deguchi *et al.* (2013); however, here we found that the nonlinear interaction only occurs in a region of vertical and spanwise length scales of $O((\alpha Re)^{-1/3})$, where α is the streamwise wavenumber. The localization of the nonlinear structure naturally creates a laminar–turbulent banded pattern. The new theory has two important properties: (i) the local nonlinear structure can be embedded in any shear flow when the basic flow is locally approximated by a linear profile; (ii) the local nonlinear structure is invariant under certain self-similar transformation, and therefore the theory can be applicable for various spatial scales. These properties are similar to those seen in the VWI theory in an unbounded domain.

The theoretical tilt angle for the BREs state is $\tan\phi \sim O(\alpha\delta)$, where $\delta \sim (\alpha Re)^{-1/3}$. For the largest-scale structure, which is the most energetic and has $\alpha \sim O(Re^{-1})$

https://doi.org/10.1017/jfm.2015.542 Published online by Cambridge University Press

and $\delta \sim O(1)$, the scaling of the tilt angle is again consistent with Barkley & Tuckerman (2007). Our numerical computations suggest that the asymptotically converged result can at least qualitatively predict the oblique exact coherent structures even for transitional Re as low as 350, which is used in the simulation by Barkley & Tuckerman (2005). The appropriately rescaled asymptotic results for $Re = 350$ are at least qualitatively reminiscent of the simulation. Therefore the essential sustainment mechanism behind the oblique banded pattern in subcritical shear flows is likely to be elucidated by the BRE-type asymptotic theory developed in this paper.

Acknowledgements

This work was supported by EPSRC grant EP/1037946/1. The authors would like to thank the referees for their helpful comments.

REFERENCES

BARKLEY, D. & TUCKERMAN, L. S. 2005 Computational study of turbulent–laminar patterns in Couette flow. *Phys. Rev. Lett.* **94**, 014502.

BARKLEY, D. & TUCKERMAN, L. S. 2007 Mean flow of turbulent–laminar patterns in plane Couette flow. *J. Fluid Mech.* **576**, 109–137.

COLES, D. 1965 Transition in circular Couette flow. *J. Fluid Mech.* **21**, 385–425.

DEGUCHI, K. & HALL, P. 2014*a* The high Reynolds number asymptotic development of nonlinear equilibrium states in plane Couette flow. *J. Fluid Mech.* **750**, 99–112.

DEGUCHI, K. & HALL, P. 2014*b* Canonical exact coherent structures embedded in high Reynolds number flows. *Phil. Trans. R. Soc. Lond.* A **372**, 20130352, 1–19.

DEGUCHI, K., HALL, P. & WALTON, A. G. 2013 The emergence of localized vortex–wave interaction states in plane Couette flow. *J. Fluid Mech.* **721**, 58–85.

DEGUCHI, K. & ALTMEYER, S. 2013 Fully nonlinear mode competitions of nearly bicritical spiral and Taylor vortices in Taylor–Couette flow. *Phys. Rev.* E **87** (4), 043017.

SCHNEIDER, T. M., GIBSON, J. F. & BURKE, J. 2010 Snakes and ladders: localized solutions of plane Couette flow. *Phys. Rev. Lett.* **104**, 104501.

HALL, P. 1985 The Görtler vortex mechanism in three-dimensional boundary layers. *Proc. R. Soc. Lond.* A **399**, 135–152.

HALL, P. & SMITH, F. T. 1991 On strongly nonlinear vortex/wave interactions in boundary-layer transition. *J. Fluid Mech.* **227**, 641–666.

HALL, P. & SHERWIN, S. 2010 Streamwise vortices in shear flows: harbingers of transition and the skeleton of coherent structures. *J. Fluid Mech.* **661**, 178–205.

BLACKBURN, H. M., HALL, P. & SHERWIN, S. 2013 Lower branch equilibria in Couette flow: the emergence of canonical stats for arbitrary shear flows. *J. Fluid Mech.* **726**, R2.

NAGATA, M. 1990 Three-dimensional finite-amplitude solutions in plane Couette flow: bifurcation from infinity. *J. Fluid Mech.* **217**, 519–527.

ITANO, T. & GENERALIS, S. C. 2009 Hairpin vortex solution in planar Couette flow: a tapestry of knotted vortices. *Phys. Rev. Lett.* **102**, 114501.

GIBSON, J. F. & BRAND, E. 2014 Spanwise-localized solutions of planar shear flows. *J. Fluid Mech.* **745**, 25–61.

GIBSON, J. F., HALCROW, J. & CVITANOVIC, P. 2009 Equilibrium and travelling-wave solutions of plane Couette flow. *J. Fluid Mech.* **638**, 1–24.

PRIGENT, A., GREĢOIRE, G., CHATÉ, H., DAUCHOT, O. & VAN SAARLOOS, W. 2002 Large-scale finite-wavelength modulation within turbulent shear flows. *Phys. Rev. Lett.* **89**, 014501.

TAYLOR, G. 1923 Stability of a viscous liquid contained between two rotating cylinders. *Phil. Trans. R. Soc. Lond.* A **A223**, 289–343.

TSUKAHARA, T., SEKI, Y. & TOCHIO, D. 2005 DNS of turbulent channel flow at very low Reynolds numbers. In *Proceedings of the 4th International Symposium on Turbulence and Shear Flow Phenomena*, pp. 935–940.

WALEFFE, F. 1997 On a self-sustaining process in shear flows. *Phys. Fluids* **9**, 883–900.

https://doi.org/10.1017/jfm.2015.542 Published online by Cambridge University Press